

Surface-Limited Superconducting Phase Transition on 1T-TaS₂

Ziying Wang,^{†,‡} Yi-Yang Sun,^{‡,§,¶} Ibrahim Abdelwahab,[†] Liang Cao,^{§,¶} Wei Yu,[†] Huanxin Ju,[⊥] Junfa Zhu,[⊥] Wei Fu,[†] Leiqiang Chu,[†] Hai Xu,^{*,†,§,¶} and Kian Ping Loh^{*,†,¶}

[†]Department of Chemistry, Centre for Advanced 2D Materials, National University of Singapore, Singapore 117543

[‡]State Key Laboratory of High Performance Ceramics and Superfine Microstructure, Shanghai Institute of Ceramics, Chinese Academy of Sciences, Shanghai 201899, China

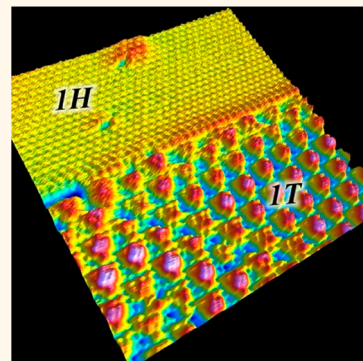
[§]Changchun Institute of Optics, Fine Mechanics and Physics, Chinese Academy of Science, Changchun 130033, China

[⊥]National Synchrotron Radiation Laboratory, University of Science and Technology of China, Hefei 230026, China

S Supporting Information

ABSTRACT: Controlling superconducting phase transition on a two-dimensional (2D) material is of great fundamental and technological interest from the viewpoint of making 2D resistance-free electronic circuits. Here, we demonstrate that a 1T-to-2H phase transition can be induced on the topmost monolayer of bulk (<100 nm thick) 1T-TaS₂ by thermal annealing. The monolayer 2H-TaS₂ on bulk 1T-TaS₂ exhibits a superconducting transition temperature (T_c) of 2.1 K, which is significantly enhanced compared to that of bulk 2H-TaS₂. Scanning tunneling microscopy measurements reveal a 3×3 charge density wave (CDW) in the phase-switched monolayer at 4.5 K. The enhanced T_c is explained by the suppressed 3×3 CDW and a charge-transfer doping from the 1T substrate. We further show that the monolayer 2H-TaS₂ could be switched back to 1T phase by applying a voltage pulse. The observed surface-limited superconducting phase transition offers a convenient way to prepare robust 2D superconductivity on bulk 1T-TaS₂ crystal, thereby bypassing the need to exfoliate monolayer samples.

KEYWORDS: 2D materials, TaS₂, superconducting, surface phase transition, charge density wave



Group-VB layered transition metal dichalcogenides (TMDs) MX₂ (M = Nb or Ta and X = S or Se) are ideal systems to explore various electronic ordering behaviors, including superconductivity and charge density waves (CDWs).^{1,2} Different from group-IVB (Zr and Hf) and group-VIB (Mo and W) TMDs that are usually semiconductors with relatively large band gaps,^{3–6} group-VB TMDs are metallic at room temperature and undergo superconducting phase transition at sufficiently low temperature. Another attractive aspect of group-VB TMDs is their vast varieties of atomic and electronic structures associated with the formation of CDWs,^{2,7–9} therefore serving as good model systems for investigating the coexistence and competition between various charge-ordered states.^{10–13} Polymorph transitions arising from different intralayer stacking in TaS₂ has been intensively researched with a view for controlling polymorph-specific properties such as metallic–insulator transition, superconductivity, and charge density wave order. In TaS₂, by a change of stacking order in response to pressure or temperature, the bulk crystal can adopt octahedral (1T), trigonal prismatic (2H), or other alternating configurations (4Hb and 6R).^{2,14,15} 1T-TaS₂ has a rich phase diagram: metal above 543 K, incommensurate charge density wave (ICCDW)

below 543 K, nearly commensurate charge density wave (NCCDW) below 350 K, and commensurate charge density wave ($\sqrt{13} \times \sqrt{13}$ CCDW) state below 200 K.^{2,8,16,17} Bulk 1T-TaS₂ does not show superconductivity except when subjected to high pressure or intercalation of extrinsic elements.^{12,18} In contrast, bulk 2H-TaS₂ develops 3×3 CDW modulation at 75 K and a superconductivity phase at 0.8 K.^{2,19,20}

Metallic layered TMD compounds offer an opportunity to realize superconductivity down to monolayer thickness. From an application perspective, a monolayer superconductor presents the alluring prospect of a dissipationless device that can be miniaturized vertically and offer potential solutions to the thermal management issues facing current silicon-based complementary metal oxide semiconductor (CMOS) technology.²¹ At the atomically thin limit, the competition between electron–phonon coupling, electron–electron interactions, and disorder provides stabilization or destabilization forces to

Received: September 27, 2018

Accepted: November 7, 2018

Published: November 7, 2018

the charge-ordered state. In particular, the microscopic formation mechanism of CDW and superconducting phases at the atomically thin limit is not well understood.^{17,18} Recent work reported that vertically scaling the thickness of 2D materials can change the superconducting transition temperature (T_c). In 2H-NbSe₂, for example, T_c was found to decrease from the bulk value of 7.2 K to between 1 and 3 K for the monolayer,^{10,11,22–24} and this has been attributed to the enhancement of electron–phonon coupling constants.²⁵ In contrast, enhanced T_c had been reported on few-layer 2H-TaS₂;^{11,25,26} a T_c of 3.4 K is reported on monolayer 2H-TaS₂, as compared to 0.8 K of the bulk crystal. The suppression of CDW order, which competes with superconducting pairing, has been proposed to be responsible for the enhanced T_c in 2H-TaS₂.²⁵

Phase-controlled synthesis of TMDs offer a strategy to fabricate metal/semiconductor or metal/superconductor transition for electronic applications.^{27,28} It is technically challenging to prepare monolayer 2H-TaS₂ by chemical vapor deposition or mechanical exfoliation; thus a reliable and scalable method for preparing a superconducting monolayer is highly desirable. A monolayer superconductor is prone to electronic instability arising from interfacial electron–phonon coupling.^{29,30} To reduce interfacial lattice strain experienced by a monolayer 2H flake on a hetero-substrate, one strategy is to create 2D superconductivity on the surface of a bulk crystal. For example, 2D superconductivity with an effective thickness of 1.5 nm has been induced on bulk MoS₂ flakes that are tens of nanometer in thickness by ionic gating.³¹

Herein, we investigate surface-limited polymorph conversion on a 1T-TaS₂ crystal that is tens of nanometer thick by exploiting the tendency for surfaces to undergo thermally induced relaxation, whereby the conversion of the surface to a monolayer 2H polymorph creates 2D superconductivity on a bulk crystal. The polymorph conversion has been verified by scanning tunneling microscopy (STM) to be restricted to the topmost layer. In addition, we performed transport measurements and found that the 2H-1T heterostructure device behaves as a metal without a Mott phase transition and exhibits a superconducting transition at 2.1 K, which is about 3 times higher than the T_c of bulk 2H-TaS₂. Our work demonstrates a simple approach to induce monolayer superconductivity on bulk crystal by allowing the surface to undergo polymorph transition, leading to an insulator–superconductor van der Waals (vdW) heterostructure.

RESULTS AND DISCUSSION

Figure 1 shows the relative stability of the 1T and 2H polymorphs for monolayer TMDs calculated using density functional theory (DFT). It is clear that the energy differences between the 1T and 2H polymorphs of group-VB TMDs are significantly smaller than those for group-IVB and group-VIB TMDs. In particular, TaS₂ possesses an energy difference of less than 0.1 eV per formula unit (f.u.) between the 1T and 2H polymorphs, which is possibly the smallest energy difference between the two polymorphs among known TMDs; thus it is chosen for this study due to the possibility of achieving facile polymorph conversion by heat or electrical energy.

Figure 2b shows the topography of an as-cleaved 1T-TaS₂ sample obtained using STM at 77.8 K. It is known that at this temperature, 1T-TaS₂ exists in the CCDW phase accompanied by a $\sqrt{13} \times \sqrt{13}$ reconstruction of the atomic lattice.^{2,8,17,32} A

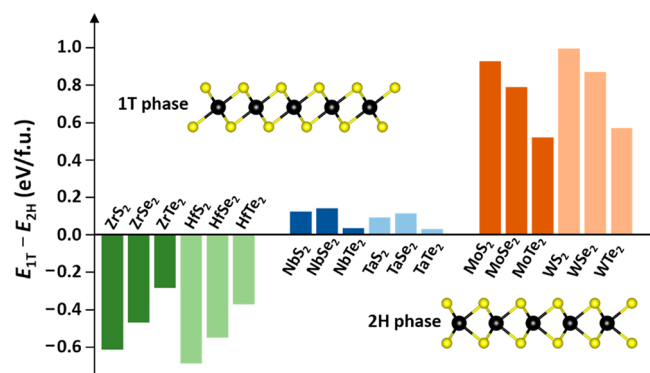


Figure 1. Energy difference between 1T and 2H polymorphs of group-IVB, VB, and VIB TMDs. Data were obtained using DFT calculation with the SCAN+rVV10 functional. While the most stable polymorphs for some of the tellurides, e.g., NbTe₂, TaTe₂, and WTe₂, are various distorted 1T polymorphs, we included these materials in the plot to illustrate the general trend.

zoom-in view in Figure 2c confirms the CCDW phase with a measured distance of about 12.1 Å between the centers of two bright spots. Figure 2d shows the differential conductance (dI/dV) spectrum on the CCDW surface (black line), which resolves two prominent peaks located at -0.24 eV (lower Hubbard band) and 0.19 eV (upper Hubbard band), respectively, thus opening a Mott gap of 0.43 eV. Beyond the lower Hubbard band, the peak at -0.35 eV is due to the top of subvalence band of TaS₂. A dip around -0.3 eV that splits the lower Hubbard peak and the valence peak is ascribed to the CDW formation. The shape of the dI/dV spectrum is consistent with previous reports of 1T-TaS₂.^{8,17}

The sample was then subjected to thermal annealing at above 250 °C in ultrahigh vacuum (UHV). Figure 2e shows the surface topography after annealing. Under the same tunneling condition, i.e., bias, current and temperature, the surface topography exhibits a significant change from that before annealing (Figure 2b). A zoom-in view in Figure 2f shows that the surface periodicity changes to 1 × 1, which we attribute to a transition to 2H polymorph because a 1 × 1 periodicity is unexpected on the surface of the 1T polymorph at this temperature. The dI/dV spectrum recorded on this 1 × 1 surface, as shown in Figure 2d (red line), reveals a metallic state with a finite density of states (DOS) around the Fermi level (E_F). The two Hubbard peaks observed on the as-cleaved 1T-TaS₂ surface disappear. In addition, a sharp peak (marked by green arrow) at -0.35 eV appears, the origins of which are due to convoluted DOS from both 2H and 1T polymorphs, according to DFT calculations (Figure 6e). It indicates that the top surface has transferred to the 2H polymorph from the original 1T, as shown in Figure 2a. A small dip in the dI/dV spectrum with shoulders at -0.1 and 0.05 V is observed, arising from the indirect gap between Ta-dz² bands near Fermi surface and higher Ta-d bands.^{33,34}

Devices were fabricated on samples before and after annealing to study the emergence of superconductivity. The resistance–temperature (R–T) curves were measured using a four-probe device configuration (Supplementary Figure S1) and displayed in Figures 3a and b. The 1T-TaS₂ sample without annealing shows a typical semiconducting behavior; that is, the resistance increases with the temperature decreasing. The sudden increase of resistivity at 185 K indicates a transition from the NCCDW to the CCDW

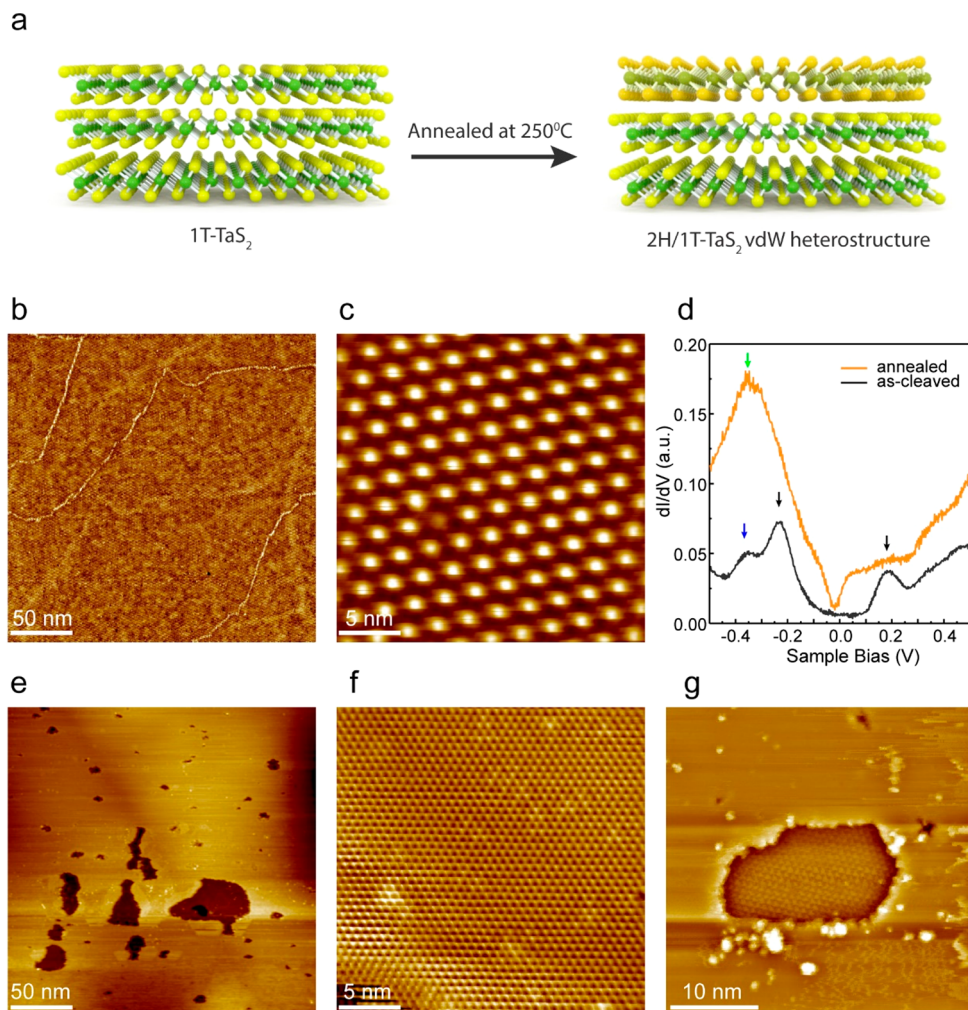


Figure 2. Polymorph transition on the 1T-TaS₂ surface by thermal annealing. (a) Schematic of a monolayer polymorph transition occurring in the topmost monolayer of 1T-TaS₂. (b) STM topography of the as-cleaved 1T-TaS₂ surface. Scale bar, 50 nm. (c) Zoom-in view of the as-cleaved 1T-TaS₂ surface showing the CCDW phase with a $\sqrt{13} \times \sqrt{13}$ periodicity. Scale bar, 5 nm. (d) dI/dV spectra recorded on the 1T-TaS₂ surface before (black) and after (red) thermal annealing. The arrow marks are discussed in the text. (e) STM topography of a 1T-TaS₂ surface after annealing at 250 °C. Scale bar, 50 nm. (f) Zoom-in view of the annealed surface showing a 1 × 1 periodicity. Scale bar, 5 nm. (g) Zoom-in view of a pit on the annealed surface showing $\sqrt{13} \times \sqrt{13}$ periodicity in the pit and 1 × 1 periodicity outside. Scale bar, 10 nm. All STM/STS data were obtained at 77.8 K.

phase.^{2,7,35} Upon heating, the reverse transition from CCDW to NCCDW exhibits a hysteresis with a transition temperature of 260 K; essentially, the R-T curve is consistent with that of 1T-TaS₂, as reported previously.^{2,12,20}

In sharp contrast, the annealed sample shows a metallic behavior; that is, the resistance decreases as temperature decreases. As shown in Figure 3b, the resistance varies linearly with temperature until T_c , which is attributed to phonon-limited resistivity and characteristic of metallic behavior. The inset of Figure 3b shows that the superconducting transition occurs at about 2.1 K. It is well known that 2H-TaS₂ presents a superconducting phase; therefore we attribute the presence of superconductivity to a 1T-to-2H surface polymorph transition. Since the 2H polymorph is far more conducting than the insulating 1T polymorph, especially at low temperature, the 2H phase dominates the electrical transport properties. It is important to note that the T_c observed here is about 3 times that of bulk 2H-TaS₂ and its R-T relation deviates from the trends reported for bulk or few-layer 2H-TaS₂ devices.^{11,20,25} The residual resistance in the superconducting phase is

nonzero; this is due to crystal imperfections in the fabricated 2H-TaS₂ monolayer.²⁶ It was reported previously that at 70 K the bulk 2H phase undergoes a quick drop in resistance, which is due to the appearance of 3×3 CDW; however such a fingerprint feature is absent in the R-T curve in Figure 3b, suggesting that the 3×3 CDW phase is suppressed to much lower temperatures.

To further characterize the electronic transport property of the 2H-1T heterostructure formed by the surface 1T-to-2H polymorph transition, an out-of-plane magnetic field was applied to the sample. Figure 3c shows the R-T curves at various perpendicular magnetic fields. T_c is gradually lowered as the field strength increases, which is a typical feature of a type-II superconductor.^{36,37} Figure 3d shows longitudinal resistance as a function of perpendicular magnetic field at various temperatures. The magnetoresistance in the superconducting range is positive. The 2H-1T heterostructure presents an upper critical field (B_{c2}) of 1.4 T at 250 mK. The 2D nature of this superconductivity can be deduced from the superconducting coherence length of monolayer 2H-TaS₂,

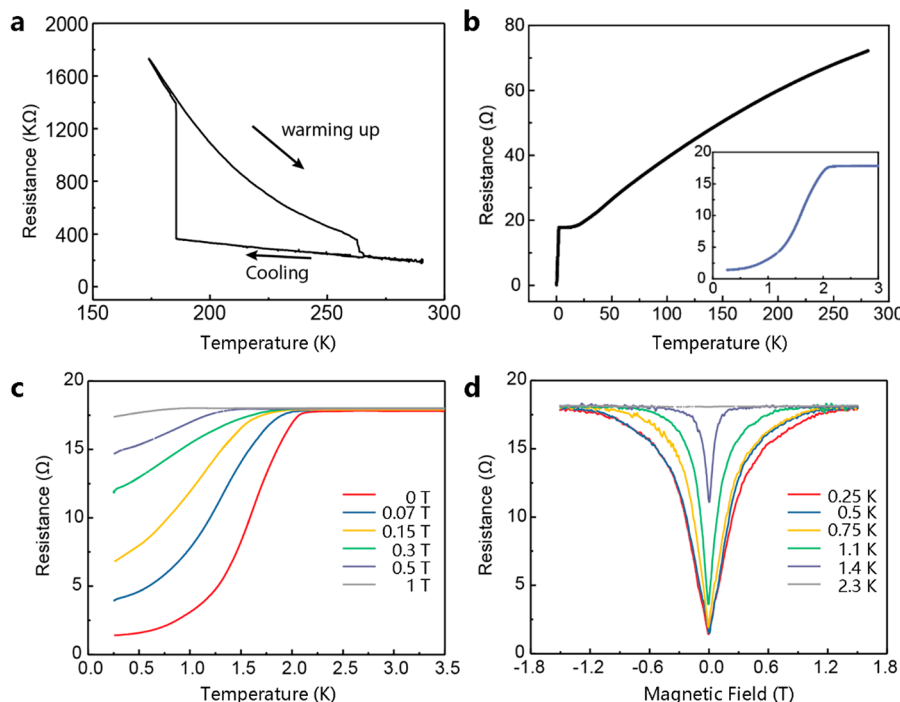


Figure 3. Electrical transport measurements of the 1T-TaS₂ samples without and with thermal annealing. (a) In-plane resistance as a function of temperature (R - T curve) of the 1T-TaS₂ sample without annealing. The NCCDW-to-CCDW phase transition occurs at 185 K, and the CCDW-to-NCCDW phase transition occurs at 260 K. (b) R - T curve recorded on the annealed 1T-TaS₂ sample showing a superconducting transition at 2.1 K, as highlighted in the inset. (c) R - T curves of annealed 1T-TaS₂ in the superconducting range under varying magnetic fields perpendicular to the surface. (d) Resistance as a function of the perpendicular magnetic field of annealed 1T-TaS₂ at varying temperatures.

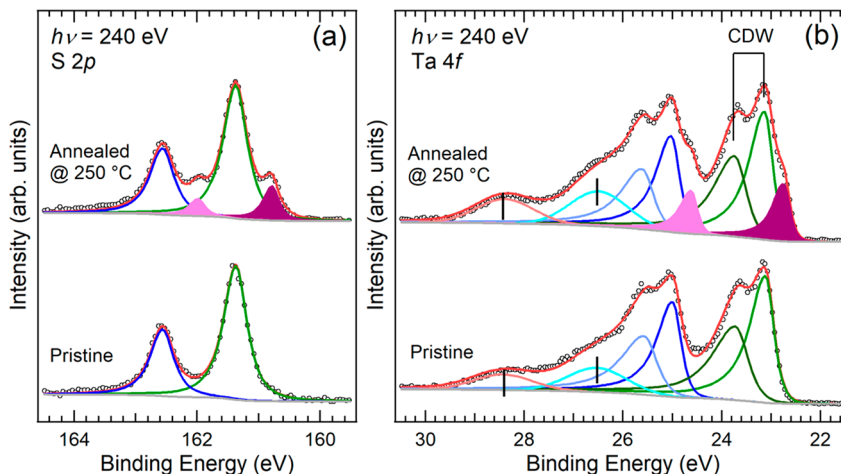


Figure 4. XPS spectra of the 1T-TaS₂ surface before and after annealing, showing the S 2p and Ta 4f core levels. As labeled in the plots, “pristine” indicates the sample before annealing, and “annealed@250 °C” indicates the plot of the sample after annealing.

which is calculated to be 15.3 nm according to the equation $B_{c2} = \frac{\varphi_0}{2\pi\xi^2}$, where $\varphi_0 \approx 2.07 \times 10^{-15}$ Wb and ξ is the superconducting Ginzburg–Landau (GL) coherence length.³⁸ This value is larger than the thickness of the monolayer 2H-TaS₂ and close to recent results reported on few-layer 2H-TaS₂ flakes,²⁶ suggesting that the superconductivity is in the 2D limit.

As bulk 1T-TaS₂ is not superconducting, the observed superconducting transition in Figure 3b should originate from the polymorph-converted monolayer 2H-TaS₂. STM imaging, which directly probes the top 1 or 2 layers of the sample

surface, provides strong evidence that a monolayer 2H-TaS₂ is created on top of the bulk 1T-TaS₂. On the annealed surface, there are broken areas (or pits) where lower layers are exposed, thus allowing the first and second layer to be differentiated. The STM line profile across the edge of the pits reveals that the height of the edge is about 0.6 nm, which is equivalent to the thickness of a TaS₂ monolayer (Supplementary Figure S2). Atomic resolution STM images within the pits show that the bottom layer preserves the $\sqrt{13} \times \sqrt{13}$ CCDW phase, whereas the topmost layer shows a 1×1 phase (see Figure 2g as well as Supplementary Figure S2 obtained on another pit from the surface).

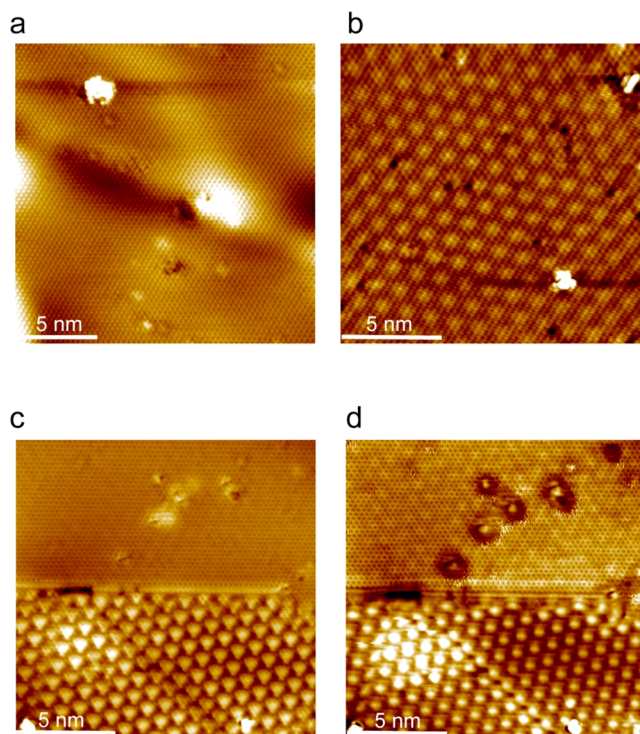


Figure 5. Polymorph transition excited by applying a tip voltage pulse in the annealed 1T-TaS₂ surface. (a) STM image of the annealed 1T-TaS₂ surface with relatively low negative bias ($V_g = -0.5$ V, $I_t = 300$ pA), showing 1×1 periodicity. (b) Similar to (a), but with a relatively high positive bias ($V_g = 1$ V, $I_t = 300$ pA), where a $\sqrt{13} \times \sqrt{13}$ superstructure is superposed on the 1×1 lattice. (c) STM image of the annealed 1T-TaS₂ surface after applying a voltage pulse of $V_g = 3$ V for 300 ms. Imaging condition is $V_g = -0.5$ V and $I_t = 300$ pA. (d) Similar to (c), but with imaging condition $V_g = 1$ V and $I_t = 300$ pA. All images in this figure were obtained at 77.8 K. Scale bar is 5 nm in all images.

Our results indicate that thermal annealing provides the activation energy for transforming the 1T to the more stable 2H phase. Under our UHV annealing condition, the phase transition is limited to the surface, due possibly to the greater ease of structural relaxation of surface atoms. Raman spectroscopy was also used to track the polymorph transition (Supplementary Figure S4). The CCDW folded-back peaks³⁹ were observed before and after annealing, indicating that the deeper layers of the crystals retained their 1T polymorph structure and were not degraded by heating, as shown in Figure S4. However, although we are able to see the 1T-to-2H polymorph transition using STM, we are not able to resolve the 2H phase clearly by Raman spectroscopy due to its surface-limited thickness and the overlap of the 2H signal with the 1T phase.^{40,41}

In order to further confirm this 1T-to-2H polymorph transition after thermal annealing, high-resolution photo-emission spectroscopy was conducted. As shown in Figure 4, the evolution of the S 2p and Ta 4f spectrum after annealing clearly shows that the 2H phase appears in the 1T-TaS₂ sample. The S 2p core-level spectrum of pristine 1T-TaS₂ shows well-resolved peaks at 161.4 (2p_{3/2}) and 162.6 eV (2p_{1/2}), which agrees well with the reported S 2p spectrum of 1T-TaS₂.⁴² After annealing at 250 °C for 2 h in UHV, new peaks at 160.8 eV (2p_{3/2}, purple) and 162.0 eV (2p_{1/2}, pink) appear, which are the signature peaks of S 2p for the 2H phase

TaS₂.⁴³ The Ta 4f core-level spectra of 1T-TaS₂ before and after annealing are shown in Figure 4b. The peaks located at 23.1, 25.0 eV, and 23.7, 25.6 eV are attributed to the CDW phase of 1T-TaS₂.⁴⁴ A new doublet component with binding energies of ~22.8 and ~24.7 eV (filled with purple and pink) is observed for the annealed sample, which is attributed to Ta⁴⁺ 4f_{7/2} and Ta⁴⁺ 4f_{5/2} of 2H-TaS₂.⁴²

To rule out that the possibility that the surface phase change we observed is due to different sample thickness or substrate effects, we have prepared samples of different thickness and placed them on either Au/Si or SiO₂/Si substrates. The results show that the phase transition is independent of sample thickness and substrate and only dependent on the annealing temperature. We also did not observe a significant increase of defect density on the TaS₂ surface before and after annealing by using STM.

Another evidence for the phase change being limited only to the topmost layer is from bias-dependent STM images on the 1×1 region (*i.e.*, away from the pits). Using different tip bias voltages, we can see through the top layer so that the $\sqrt{13} \times \sqrt{13}$ CCDW phase in the second layer can be imaged simultaneously with the 1×1 phase of the topmost layer. As shown in Figure 5a and b, only a 1×1 surface structure is observed on the top 2H polymorph at a low negative bias using STM. At high positive tip bias, the 1×1 surface structure is overlapped by a $\sqrt{13} \times \sqrt{13}$ CDW arising from the underlying 1T polymorph.

To switch off the superconducting state of the 2H monolayer, an external stimulus is necessary. Applying a voltage pulse by an STM tip had been found to induce the 2H-to-1T polymorph transition;⁴⁵ similarly, we observed that a bias voltage above +2.5 V can induce a 2H-to-1T polymorph transition. The effective area of the polymorph transition depends on the applied voltage. As shown in Figure 5c and d, after a voltage pulse, two distinct polymorphs, with unit cells of $\sqrt{13} \times \sqrt{13}$ and 1×1 periodicity, respectively, and separated by a domain boundary can be clearly resolved in the STM image. Our work hints at the possibility of inducing a global 2H-to-1T phase transition by driving an electrical current through the sample, which would be ideal for achieving controlled switching between the non-superconducting and superconducting phases.

To understand the energetics of the thermally induced phase transition, it is instructive to calculate the enthalpy of formation for monolayer TaS₂ in 1T and 2H polymorphs, with and without CDWs. The $\sqrt{13} \times \sqrt{13}$ CDW of the 1T polymorph is characterized by a Star-of-David-shaped atomic lattice,³² as shown in Figure 6a. For the 2H polymorph, however, the 3×3 CDW is only observed at temperatures below 77 K.^{25,46} Our DFT calculations reveal that free-standing monolayer 2H-TaS₂ with 1×1 structure is 88 meV/f.u. more stable than the 1T polymorph. Although the $\sqrt{13} \times \sqrt{13}$ CDW reconstruction, as shown in Figure 6a, significantly lowers the energy of the 1T polymorph by about 58 meV/f.u., its energy is still higher than the 2H polymorph. The 2H polymorph could be further stabilized by about 13 meV/f.u. through the formation of the 3×3 CDW,⁴⁷ and the one with the lowest energy is shown in Figure 6a, where the longest and shortest Ta-Ta distances are 3.44 and 3.15 Å, respectively, compared to 3.32 Å in the case of the 1×1 structure. Taken together, our calculation suggests that the 2H polymorph is lower in energy than the 1T polymorph by about

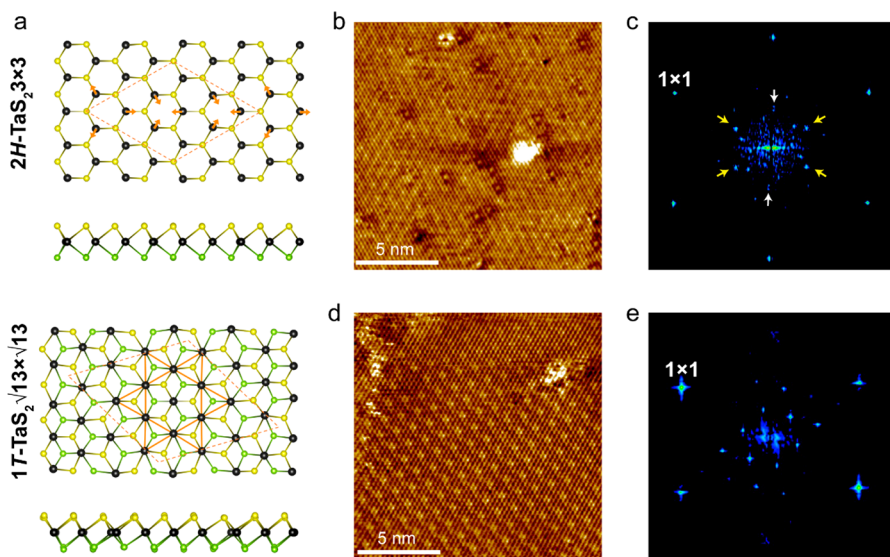


Figure 6. CDWs of the annealed 1T-TaS₂ surface at different temperatures. (a) Top and side views of atomic structures of the 3 × 3 2H polymorph and the $\sqrt{13} \times \sqrt{13}$ 1T polymorph. Arrows in the top view of the 3 × 3 2H polymorph show the directions of the atomic displacements. Brown-colored lines in the top view of the $\sqrt{13} \times \sqrt{13}$ 1T polymorph show the so-called Star of David, in which all atoms move toward the center of the star. (b) STM topography of annealed 1T-TaS₂ obtained at 4.5 K ($V_g = -0.4$ V, $I_t = 400$ pA), showing a 3 × 3 periodicity. Scale bar, 5 nm. (c) FFT image of (b). The outmost six spots are due to the 1 × 1 periodicity. The spots due to the 3 × 3 periodicity are marked by arrows, four of which are yellow-colored, indicating the strong spots, and two of which are white-colored, indicating the weak spots. (d) STM topography of annealed 1T-TaS₂ obtained at 10 K ($V_g = -0.4$ V, $I_t = 400$ pA). Scale bar, 5 nm. (e) FFT image of (d) showing clearly the $\sqrt{13} \times \sqrt{13}$ periodicity.

43 meV/f.u. Including spin-orbit coupling (SOC) in the calculations produced the same results. Since the 2H polymorph is more thermodynamically stable than 1T, these results explain why annealing bulk 1T crystal in a vacuum activates the transition to 2H.

The coexistence of superconductivity and CDW provides important clues to the mechanism for enhanced T_c .^{48–50} Given the competition between CDW and the superconducting phase, increasing T_c by suppressing CDW is one of the most significant challenges in high- T_c superconductivity research, for which similar strategies have been applied on TMDs.^{25,51} The formation of the $\sqrt{13} \times \sqrt{13}$ CCDW in the 1T polymorph opens a wide band gap and prohibits superconductivity. In the case of the 2H polymorph, while the DOS at the Fermi level is significantly reduced by the formation of the 3 × 3 CDW, it is still finite^{14,19,25,52} (Supplementary Figure S3). It has been proposed that in few-layer 2H samples the CDW is suppressed, which leads to enhanced T_c . The main evidence of CDW suppression is based on the vanishing of the commonly observed turning point in the $R-T$ curve at around 77 K as the thickness scales to the 2D limit.^{11,25,26} However, in atomically thin 2H-TaS₂, the relationship between the 3 × 3 CDW and the superconducting phase is not clear.²⁵ We did not observe the 3 × 3 CDW on the surface-switched superconducting sample at 77.8 K by STM at first. However, lowering the temperature to 4.5 K causes the 3 × 3 CDW phase to emerge, as shown in Figure 6b, where a weak 3 × 3 superstructure overlapping on a 1 × 1 2H surface can be seen. The periodicity of this superstructure can be resolved by a Fourier transform of the STM image, as shown in Figure 6c, where other than the six 1 × 1 spots, extra spots due to a 3 × 3 periodicity, as marked by arrows, can be clearly identified. The direct observation of 3 × 3 CDW down to 4.5 K suggests the possible coexistence of superconductivity and CDW in monolayer 2H-TaS₂.

Once the sample temperature is increased to ~10 K, the 3 × 3 CDW disappears, as shown in Figure 6d, and only the $\sqrt{13} \times \sqrt{13}$ lattice spots, originating from the second layer, can be observed in the Fourier transform in Figure 6e. This result suggests a significantly lower CDW transition temperature than that in bulk 2H-TaS₂. The formation of CDWs typically reduces the DOS near E_F . In the 1T-phase, the DOS will be reduced to zero; that is, a gap opens, which completely suppresses the superconductivity.²⁵ In the 2H phase, the DOS at E_F is still finite, which is responsible for the observed T_c . Our observation of a partly suppressed 3 × 3 CDW is consistent with the enhanced T_c .

To study the electronic coupling between monolayer 2H-TaS₂ on the 1T-TaS₂ substrate, a model was built for DFT calculations, in which the substrate is made of two layers of 1T-TaS₂, both of which are in the $\sqrt{13} \times \sqrt{13}$ CDW phase with the star centers aligned. A monolayer of 2H-TaS₂ with the 1 × 1 lattice structure is allowed to adsorb on top of the bilayer 1T substrate, as shown schematically in Figure 7a. Figure 7d and e show the calculated band structure and density of states of the 2H-1T heterostructure, respectively. Figure 7e shows the DOS projection onto the 2H monolayer and the 1T substrate, where only the Ta 5d components are shown because they dominate the electronic structure near E_F (set as 0 eV). The calculated DOS is consistent with the STS measurement shown in Figure 2d, revealing a dip near E_F , a sharp increase below E_F with a peak at -0.3 eV, and a small increase above E_F . It can be seen that the Ta 5d DOS states in the 2H monolayer (the blue dots in Figure 7d and the blue line in Figure 7e) mainly spread from -0.5 eV to about +1.3 eV. By analyzing the charge densities, we can identify that the d band of the 2H monolayer is contributed by the d_{z^2} states. There are clear energy gaps that separate the d_{z^2} band from higher and lower bands. Due to the narrowness of the d_{z^2} band, STM or STS measurement samples the 2H monolayer only when the bias is in the region of about

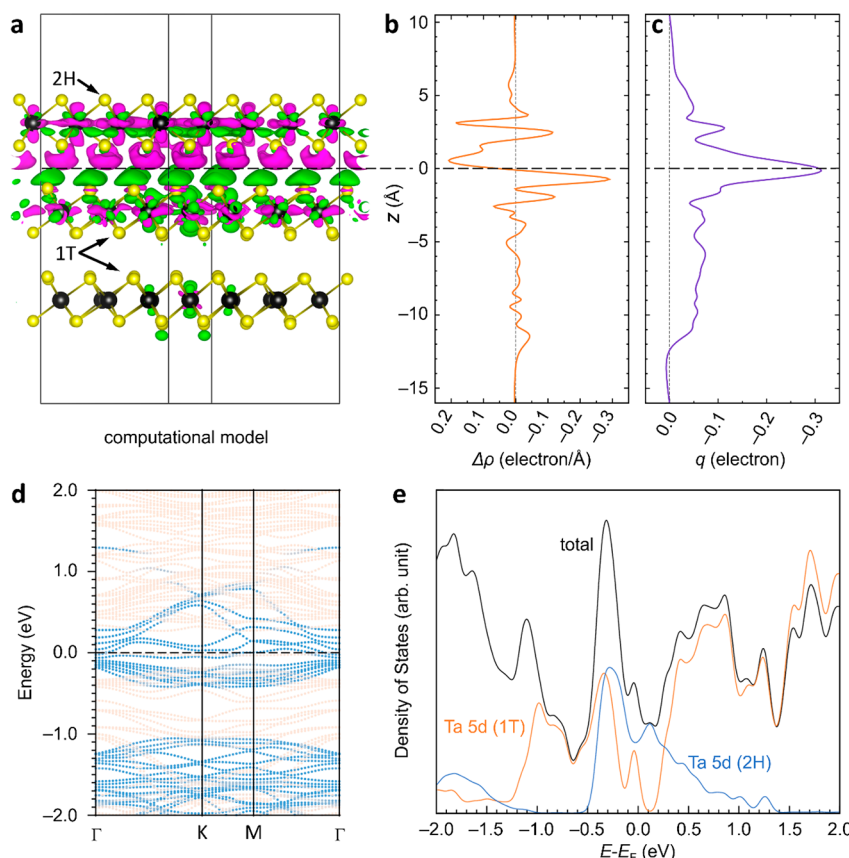


Figure 7. Electronic structure of the 2H-1T TaS₂ vdW heterostructure and charge transfer doping across the interface. (a) Atomic structure of the model system used to simulate one monolayer of 2H-TaS₂ on the bilayer 1T-TaS₂ substrate. The structure was relaxed using the SCAN-rVV10 functional. The isosurfaces show the charge density difference, where the green color represents charge deficiency and the purple color represents charge excess. (b) Charge density difference (see text) averaged in the $x-y$ basal plane. (c) Integrated charge difference from the bottom of the supercell (*i.e.*, at $z = -16 \text{ \AA}$). (d) Band structure and (e) DOS of the model 2H-1T TaS₂ vdW heterostructure in (a). In the band structure plot, each state is projected onto the 1T substrate and the 2H monolayer. States with larger projection on the 2H monolayer or 1T substrate are plotted in blue or light brown color, respectively. Similarly, the projections of DOS on the Ta 5d states in the 2H monolayer and 1T substrate are shown by blue and brown lines, respectively. The dashed line in (b), (c), and (d), which extends into (a), marks the center of the vdW gap between the substrate and the 2H monolayer, which is taken as the interface.

-0.5 to about +0.5 eV, beyond which the electronic states from the 1T substrate will dominate the spectrum. This explains that at high bias (either positive or negative) the topmost 2H monolayer TaS₂ becomes “transparent” and STM can see through the top layer and resolve the $\sqrt{13} \times \sqrt{13}$ CDW from the second layer, as shown in Figure 5b and d.¹⁵

Another possible T_c enhancement mechanism is the charge doping from the substrate,^{53,54} which has been proposed to be crucial for a monolayer FeSe high- T_c superconductor.^{29,30} Electron doping was also reported to suppress CDW in TMDs.⁵⁵ In general, excess charge could influence phase stability in TMDs. For example, electrostatic doping of 2H phase TaSe₂ can lead to a structural phase transition to the 1T phase.⁵⁶ Similar transitions can also be induced by STM tips.^{45,57} Our DFT calculations of monolayer 1T- and 2H-TaS₂ show that 1T-TaS₂ has a significantly smaller work function (5.35 eV for the $\sqrt{13} \times \sqrt{13}$ CDW phase) than that of 2H-TaS₂ (6.07 eV for the 3×3 CDW phase). This difference results in electron doping from the 1T substrate to the topmost 2H monolayer, as shown in Figure 7b and c. To verify the presence of charge transfer, we calculate the difference of the charge densities of the whole system and the separated 1T substrate and 2H top layer by $\Delta\rho = \rho_{\text{tot}} - \rho_{\text{sub}} = \rho_{\text{tot}} - \rho_{1T-\text{sub}} - \rho_{2H-\text{top}}$ where ρ_{tot} , $\rho_{1T-\text{sub}}$, and $\rho_{2H-\text{top}}$ are plane-averaged (in

the $x-y$ basal plane) charge densities of the whole model, the 1T substrate, and the 2H top layer, respectively. $\rho_{1T-\text{sub}}$ and $\rho_{2H-\text{top}}$ were calculated by removing the 2H monolayer and the 1T substrate, respectively, while maintaining the atomic structures unchanged. As can be seen in Figure 7b, on the 1T substrate side (*i.e.*, the part lower than the horizontal dashed line), there is an overall charge density reduction, while in the 2H monolayer there is a charge density accumulation. This charge transfer can also be visualized in the plot of charge density difference in Figure 7a, where the green color isosurface represents charge deficiency and the purple color represents charge excess. Figure 7c shows the integrated charge (q) from the bottom of the supercell (*i.e.*, from about $z = -16 \text{ \AA}$). At the interface between the 1T substrate and 2H top layer (*i.e.*, at $z = 0 \text{ \AA}$), the total charge deficiency from the 1T substrate (*i.e.*, the total transferred charge to the 2H monolayer) is about 0.31 electron per $\sqrt{13} \times \sqrt{13}$ cell.

CONCLUSION

We have discovered that a 1T-to-2H polymorph transition can be induced on the surface of bulk 1T-TaS₂ (<100 nm thick) simply by thermal annealing. The relaxation is most pronounced at the surface due to larger freedom for atom displacement, which allows the thermodynamically more stable

2H polymorph to manifest. STM measurement confirms that the transition to 2H-TaS₂ occurs in the topmost layer only, thus affording a surface-confined 2D superconductivity with a T_c of 2.1 K, which is significantly enhanced from that of the bulk 2H crystal. STM measurement further evidences that the 3×3 CDW phase is suppressed and exists at 4.5 K in the 2H monolayer, which could be correlated to the enhanced T_c . DFT calculation reveals the presence of transfer doping of electrons from the 1T substrate to the 2H monolayer, which may contribute to the enhanced T_c . Our work provides a simple method to fabricate a CDW Mott-insulator/superconductor vdW heterostructure, which could serve as a platform to study the proximity effect of CDW on superconductivity.

METHODS

STM/STS Measurements. Our experiments were performed in an Omicron UHV system containing a sample preparation chamber (base pressure below 5×10^{-10} mbar) and an analysis chamber (base pressure below 2×10^{-11} mbar) equipped with a low-temperature STM. To avoid surface contamination in the air, a freshly cleaved 1T-TaS₂ sample was quickly transferred into the preparation chamber. The sample was annealed at about 200–250 °C for 2–3 h by applying a dc current and then cooled to room temperature before transferring to the analysis chamber to carry out STM experiment. STS measurements were performed in constant-height mode using standard lock-in technique ($f = 773.1$ Hz, $V_{rms} = 16$ mV). The dI/dV spectrum taken on a Au(111) surface was used as the reference for tip calibration.

Transport Measurement. For transport measurements, the devices were fabricated by the standard electron beam lithography process using poly(methyl methacrylate) (PMMA) as positive resist. Electrodes were deposited through thermal deposition of Cr (5 nm)/Au (65 nm), as shown in Figure S1. A thin h-BN flake (~20 nm) was transferred on top of the test samples in a nitrogen-filled glovebox as an encapsulation layer to avoid oxidation in the air during measurements. Low-temperature transport measurements were performed in a 4He cryostat and a 3He/4He dilution cryostat with a standard four-probe setup.

XPS Measurements. High-resolution photoemission spectroscopy (PES) was performed using the beamline facilities in the National Synchrotron Radiation Laboratory (NSRL, China). All the measurements were performed at room temperature in a UHV chamber equipped with a Scienta R4000 electron energy analyzer and with a base pressure of 1×10^{-10} mbar. The S 2p and Ta 4f spectra were measured using 240 eV photon energy with an energy resolution of 24 meV and a beam spot size of $0.2(H) \times 0.1(V)$ mm². The photon energy was calibrated using the Au 4f_{7/2} core-level peak (84.0 eV) of gold foil in electrical contact with the sample. The least-squares peak fit was performed employing a Shirley background subtraction, asymmetric peak profiles for TaS₂ species, and Voigt photoemission profiles with constant Lorentzian (10%) and Gaussian (90%) line shapes for TaO_x species. For S 2p and Ta 4f doublets, the spin-orbit splitting differences of ~1.19 eV with a branching ratio of 2 (2 p_{3/2}):1 (2 p_{1/2}) and ~1.88 eV with a branching ratio of 8 (4 f_{7/2}): 6 (4 f_{5/2}) were used for peak fitting, respectively. The full width at half-maximum for each doublet was fixed during the peak-fitting process. The 1T-TaS₂ flake samples were prepared in a glovebox and directly adhered on molybdenum sample holders by gentle pressure; then the sample was transferred quickly to a PES chamber within a few of minutes of air expose. The annealing process was carried out in an adjoined UHV preparation chamber (base pressure $< 5 \times 10^{-10}$ mbar).

Raman Measurements. An NT-MDT Raman spectroscopy system with a 633 nm He-Ne wavelength laser was employed to conduct a low-temperature Raman measurement. The laser was focused on the sample through a 50× objective, with a 1 μm spot size. The sample was mounted in a sealed temperature chamber, with a pressure below 1×10^{-2} Torr to minimize oxidation and to ensure

effective cooling during the measurement. The measurement temperature can be lowered to 78 K in a cold-hot cell with a temperature stability of ±0.1 K.

DFT Calculation. Our calculations were performed using the Vienna *ab Initio* Simulation Package (VASP) employing a planewave basis set. We used the strongly constrained and appropriately normed (SCAN) exchange-correlation functional amended by the rVV10 functional for the vdW interaction. The ion cores were represented by the projector-augmented wave (PAW) potentials. The kinetic cutoff energy for the planewaves was set to 40 Ry; $18 \times 18 \times 1$, $6 \times 6 \times 1$, and $5 \times 5 \times 1$ k-point grids were used for the (1 × 1), (3 × 3), and ($\sqrt{13} \times \sqrt{13}$) supercells, respectively. Structural optimizations were carried out until the force on each atom was smaller than 0.5 mRy/Bohr. Spin-orbit interaction was added to the all-electron part of the PAW Hamiltonian by a variational treatment in VASP.

ASSOCIATED CONTENT

Supporting Information

The Supporting Information is available free of charge on the ACS Publications website at DOI: [10.1021/acsnano.8b07379](https://doi.org/10.1021/acsnano.8b07379).

Sample preparation for 1T-TaS₂ flakes; low-temperature Raman characterization for a 1T-TaS₂ flake before and after annealing ([PDF](#))

AUTHOR INFORMATION

Corresponding Authors

*E-mail: phyxuh@gmail.com.

*E-mail: chmlohp@nus.edu.sg.

ORCID

Yi-Yang Sun: [0000-0002-0356-2688](https://orcid.org/0000-0002-0356-2688)

Ibrahim Abdelwahab: [0000-0002-0107-5827](https://orcid.org/0000-0002-0107-5827)

Liang Cao: [0000-0001-7453-7060](https://orcid.org/0000-0001-7453-7060)

Junfa Zhu: [0000-0003-0888-4261](https://orcid.org/0000-0003-0888-4261)

Hai Xu: [0000-0002-4047-7087](https://orcid.org/0000-0002-4047-7087)

Kian Ping Loh: [0000-0002-1491-743X](https://orcid.org/0000-0002-1491-743X)

Author Contributions

#Z. Wang and Y.-Y. Sun contributed equally to this work.

Author Contributions

H.X. and K.P.L. conceived the project. Z.W., I.A., and L.Chu prepared the devices and performed transport. Y.Y.S. performed the DFT calculations. H.X., L.Cao, and Y.W. carried out PES measurement and performed data analysis. H.X. and Z.W. performed STM experiments. H.X., Y.Y.S., Z.W., and K.P.L. wrote the paper. Z.W. and L.Chu performed Raman measurements. W.F. drew the illustration in Figure 2a. All authors contributed to the data analysis and read the manuscript.

Notes

The authors declare no competing financial interest.

ACKNOWLEDGMENTS

K.P.L. acknowledges support from National Research Foundation, Prime Minister's office, Midsized Centre Fund. Y.Y.S. and L.C. acknowledge support from the National Natural Science Foundation of China (Grant Nos. 11774365, 11574317, and 21503233). L.C. acknowledges project support by the State Key Laboratory of Luminescence and Applications (Grant No. SKLA-2018-02). The authors thank beamline BL11U at NSRL for providing the beam time. H.X. thanks the support from the National Natural Science Foundation of China (Grant No. 11774341) and the 100 Talents Program of the Chinese Academy of Sciences.

REFERENCES

- (1) Foner, S.; McNiff, E. J. Upper Critical Fields of Layered Superconducting NbSe₂ at Low Temperature. *Phys. Lett. A* **1973**, *45*, 429–430.
- (2) Wilson, J. A.; Di Salvo, F. J.; Mahajan, S. Charge-Density Waves and Superlattices in the Metallic Layered Transition Metal Dichalcogenides. *Adv. Phys.* **1975**, *24*, 117–201.
- (3) Mak, K. F.; Lee, C.; Hone, J.; Shan, J.; Heinz, T. F. Atomically Thin MoS₂: A New Direct-Gap Semiconductor. *Phys. Rev. Lett.* **2010**, *105*, 136805.
- (4) Jones, A. M.; Yu, H.; Ghimire, N. J.; Wu, S.; Aivazian, G.; Ross, J. S.; Zhao, B.; Yan, J.; Mandrus, D. G.; Xiao, D.; Yao, W. Optical Generation of Excitonic Valley Coherence in Monolayer WSe₂. *Nat. Nanotechnol.* **2013**, *8*, 634.
- (5) Wang, Q. H.; Kalantar-Zadeh, K.; Kis, A.; Coleman, J. N.; Strano, M. S. Electronics and Optoelectronics of Two-Dimensional Transition Metal Dichalcogenides. *Nat. Nanotechnol.* **2012**, *7*, 699.
- (6) Li, Y.; Kang, J.; Li, J. Indirect-to-Direct Band Gap Transition of the ZrS₂ Monolayer by Strain: First-Principles Calculations. *RSC Adv.* **2014**, *4*, 7396–7401.
- (7) Tsen, A. W.; Hovden, R.; Wang, D.; Kim, Y. D.; Okamoto, J.; Spoth, K. A.; Liu, Y.; Lu, W.; Sun, Y.; Hone, J. C.; Kourkoutis, L. F.; Kim, P.; Pasupathy, A. N. Structure and Control of Charge Density Waves in Two-Dimensional 1T-TaS₂. *Proc. Natl. Acad. Sci. U. S. A.* **2015**, *112*, 15054–15059.
- (8) Ma, L.; Ye, C.; Yu, Y.; Lu, X. F.; Niu, X.; Kim, S.; Feng, D.; Tománek, D.; Son, Y.-W.; Chen, X. H.; Zhang, Y. B. A Metallic Mosaic Phase and the Origin of Mott-Insulating State in 1T-TaS₂. *Nat. Commun.* **2016**, *7*, 10956.
- (9) Chatterjee, U.; Zhao, J.; Iavarone, M.; Di Capua, R.; Castellan, J. P.; Karapetrov, G.; Malliakas, C. D.; Kanatzidis, M. G.; Claus, H.; Ruff, J. P. C.; Weber, F. Emergence of Coherence in the Charge-Density Wave State of 2H-NbSe₂. *Nat. Commun.* **2015**, *6*, 6313.
- (10) Xi, X.; Wang, Z.; Zhao, W.; Park, J.-H.; Law, K. T.; Berger, H.; Forró, L.; Shan, J.; Mak, K. F. Ising Pairing in Superconducting NbSe₂ Atomic layers. *Nat. Phys.* **2016**, *12*, 139.
- (11) de la Barrera, S. C. S.; Sinko, M. R.; Gopalan, D. P.; Sivadas, N.; Seyler, K. L.; Watanabe, K.; Taniguchi, T.; Tsen, A. W.; Xu, X.; Xiao, D. Tuning Ising Superconductivity With Layer and Spin-Orbit Coupling in Two-Dimensional Transition-Metal Dichalcogenides. *Nat. Commun.* **2018**, *9*, 1427.
- (12) Sipos, B.; Kusmartseva, A. F.; Akrap, A.; Berger, H.; Forró, L.; Tuttiš, E. From Mott State to Superconductivity in 1T-TaS₂. *Nat. Mater.* **2008**, *7*, 960.
- (13) Stojchevska, L.; Vaskivskyi, I.; Mertelj, T.; Kusar, P.; Svetin, D.; Brazovskii, S.; Mihailovic, D. Ultrafast Switching to a Stable Hidden Quantum State in an Electronic Crystal. *Science* **2014**, *344* (6180), 177–180.
- (14) Meyer, S. F.; Howard, R. E.; Stewart, G. R.; Acrivos, J. V.; Geballe, T. H. Properties of Intercalated 2H-NbSe₂, 4hb-TaS₂, and 1T-TaS₂. *J. Chem. Phys.* **1975**, *62*, 4411–4419.
- (15) Ekwall, I.; Kim, J.-J.; Olin, H. a. Atomic and Electronic Structures of the Two Different Layers in 4hb-TaS₂ at 4.2 K. *Phys. Rev. B: Condens. Matter Phys.* **1997**, *55*, 6758–6761.
- (16) Svetin, D.; Vaskivskyi, I.; Brazovskii, S.; Mihailovic, D. Three-Dimensional Resistivity and Switching between Correlated Electronic States in 1T-TaS₂. *Sci. Rep.* **2017**, *7*, 46048.
- (17) Cho, D.; Cheon, S.; Kim, K.-S.; Lee, S.-H.; Cho, Y.-H.; Cheong, S.-W.; Yeom, H. W. Nanoscale Manipulation of the Mott Insulating State Coupled to Charge Order in 1T-TaS₂. *Nat. Commun.* **2016**, *7*, 10453.
- (18) Yu, Y.; Yang, F.; Lu, X. F.; Yan, Y. J.; Cho, Y.-H.; Ma, L.; Niu, X.; Kim, S.; Son, Y.-W.; Feng, D.; Li, S. Gate-Tunable Phase Transitions in Thin Flakes of 1T-TaS₂. *Nat. Nanotechnol.* **2015**, *10*, 270.
- (19) Salvo, F. J. D.; Schwall, R.; Geballe, T. H.; Gamble, F. R.; Osiecki, J. H. Superconductivity in Layered Compounds with Variable Interlayer Spacings. *Phys. Rev. Lett.* **1971**, *27*, 310–313.
- (20) Coleman, R. V.; Giambattista, B.; Hansma, P. K.; Johnson, A.; McNairy, W. W.; Slough, C. G. Scanning Tunnelling Microscopy of Charge-Density Waves in Transition Metal Chalcogenides. *Adv. Phys.* **1988**, *37*, 559–644.
- (21) Kim, K.; Choi, J.-Y.; Kim, T.; Cho, S.-H.; Chung, H.-J. A Role for Graphene in Silicon-Based Semiconductor Devices. *Nature* **2011**, *479*, 338.
- (22) Frindt, R. F. Superconductivity in Ultrathin NbSe₂ Layers. *Phys. Rev. Lett.* **1972**, *28*, 299–301.
- (23) Wang, H.; Huang, X.; Lin, J.; Cui, J.; Chen, Y.; Zhu, C.; Liu, F.; Zeng, Q.; Zhou, J.; Yu, P.; Wang, X. High-Quality Monolayer Superconductor NbSe₂ Grown by Chemical Vapour Deposition. *Nat. Commun.* **2017**, *8*, 394.
- (24) Pan, J.; Guo, C.; Song, C.; Lai, X.; Li, H.; Zhao, W.; Zhang, H.; Mu, G.; Bu, K.; Lin, T.; Xie, X. Enhanced Superconductivity in Restacked TaS₂ Nanosheets. *J. Am. Chem. Soc.* **2017**, *139*, 4623–4626.
- (25) Yang, Y. F.; Fatemi, V.; Ruhman, J.; Navarro-Moratalla, E.; Watanabe, K.; Taniguchi, T.; Kaxiras, E.; Jarillo-Herrero, P. Enhanced Superconductivity and Suppression of Charge-Density Wave Order in 2H-TaS₂ in the Two-Dimensional Limit. *arXiv preprint arXiv:1711.00079* **2017**.
- (26) Navarro-Moratalla, E.; Island, J. O.; Manas-Valero, S.; Pinilla-Cienfuegos, E.; Castellanos-Gómez, A.; Quereda, J.; Rubio-Bollinger, G.; Chirolli, L.; Silva-Guillen, J. A.; Agrait, N.; Steele, G. A. Enhanced Superconductivity in Atomically Thin TaS₂. *Nat. Commun.* **2016**, *7*, 11043.
- (27) Rui, Z.; Benjamin, G.; Ram Krishna, G.; Stephen, H.; Baoming, W.; Ke, W.; Natalie, B.; Aman, H.; Suman, D.; Joshua, R. Two-Dimensional Tantalum Disulfide: Controlling Structure and Properties via Synthesis. *2D Mater.* **2018**, *5*, 025001.
- (28) Nakata, Y.; Yoshizawa, T.; Sugawara, K.; Umemoto, Y.; Takahashi, T.; Sato, T. Selective Fabrication of Mott-Insulating and Metallic Monolayer TaSe₂. *ACS Appl. Nano Mater.* **2018**, *1*, 1456–1460.
- (29) Lee, J. J.; Schmitt, F. T.; Moore, R. G.; Johnston, S.; Cui, Y. T.; Li, W.; Yi, M.; Liu, Z. K.; Hashimoto, M.; Zhang, Y.; Lu, D. H. Interfacial Mode Coupling as the Origin of the Enhancement of Tc in FeSe Films on SrTiO₃. *Nature* **2014**, *515*, 245.
- (30) Fan, Q.; Zhang, W. H.; Liu, X.; Yan, Y. J.; Ren, M. Q.; Peng, R.; Xu, H. C.; Xie, B. P.; Hu, J. P.; Zhang, T.; Feng, D. L. Plain S-Wave Superconductivity in Single-Layer FeSe on SrTiO₃ Probed by Scanning Tunneling Microscopy. *Nat. Phys.* **2015**, *11*, 946.
- (31) Saito, Y.; Nakamura, Y.; Bahramy, M. S.; Kohama, Y.; Ye, J.; Kasahara, Y.; Nakagawa, Y.; Onga, M.; Tokunaga, M.; Nojima, T.; Yanase, Y. Superconductivity Protected by Spin-Valley Locking in Ion-Gated MoS₂. *Nat. Phys.* **2016**, *12*, 144.
- (32) Brouwer, R.; Jellinek, F. The Low-Temperature Superstructures of 1T-TaSe₂ and 2H-TaSe₂. *Physica B+C* **1980**, *99*, 51–55.
- (33) Blaha, P. Electronic Structure and Electric Field Gradients in 2H-TaS₂, LiTaS₂, and SnTaS₂. *J. Phys.: Condens. Matter* **1991**, *3*, 9381.
- (34) Guo, G. Y.; Liang, W. Y. Electronic Structures of Intercalation Complexes of the Layered Compound 2H-TaS₂. *J. Phys. C: Solid State Phys.* **1987**, *20*, 4315.
- (35) Thomson, R. E.; Burk, B.; Zettl, A.; Clarke, J. Scanning Tunneling Microscopy of the Charge-Density-Wave Structure in 1T-TaS₂. *Phys. Rev. B: Condens. Matter Mater. Phys.* **1994**, *49*, 16899–16916.
- (36) Chandrasekhar, B. S. A Note on the Maximum Critical Field of High-Field Superconductors. *Appl. Phys. Lett.* **1962**, *1*, 7–8.
- (37) Clogston, A. M. Upper Limit for the Critical Field in Hard Superconductors. *Phys. Rev. Lett.* **1962**, *9*, 266–267.
- (38) Haviland, D. B.; Liu, Y.; Goldman, A. M. Onset of Superconductivity in the Two-Dimensional Limit. *Phys. Rev. Lett.* **1989**, *62*, 2180–2183.
- (39) Sugai, S.; Murase, K.; Uchida, S.; Tanaka, S. Comparison of the Soft Modes in Tantalum Dichalcogenides. *Physica B+C* **1981**, *105*, 405–409.

- (40) Sugai, S.; Murase, K.; Uchida, S.; Tanaka, S. Studies of Lattice Dynamics in 2H-TaS₂ by Raman Scattering. *Solid State Commun.* **1981**, *40*, 399–401.
- (41) Sugai, S. Lattice Vibrations in the Charge-Density-Wave States of Layered Transition Metal Dichalcogenides. *Phys. Status Solidi B* **1985**, *129*, 13–39.
- (42) Tison, Y.; Martinez, H.; Baraille, I.; Loudet, M.; Gonbeau, D. X-Ray Photoelectron Spectroscopy and Scanning Tunneling Microscopy Investigations of the Solid Solutions Ti_xTa_{1-x}S₂ (0≤X≤1). *Surf. Sci.* **2004**, *563*, 83–98.
- (43) Eppinga, R.; Sawatzky, G. A.; Haas, C.; Bruggen, C. F. V. Photoelectron Spectra of 2H-TaS₂ and Sn_xTaS₂. *J. Phys. C: Solid State Phys.* **1976**, *9*, 3371.
- (44) Hughes, H. P.; Pollak, R. A. Charge Density Waves in Layered Metals Observed by X-Ray Photoemission. *Philos. Mag.* **1976**, *34*, 1025–1046.
- (45) Zhang, J.; Liu, J.; Huang, J. L.; Kim, P.; Lieber, C. M. Creation of Nanocrystals through a Solid-Solid Phase Transition Induced by an Stm Tip. *Science* **1996**, *274*, 757–760.
- (46) Yoshida, M.; Ye, J.; Zhang, Y.; Imai, Y.; Kimura, S.; Fujiwara, A.; Nishizaki, T.; Kobayashi, N.; Nakano, M.; Iwasa, Y. Extended Polymorphism of Two-Dimensional Material. *Nano Lett.* **2017**, *17*, 5567–5571.
- (47) Wilson, J. A. More Concerning CdW Phasing in 2H-TaSe₂. *J. Phys. F: Met. Phys.* **1985**, *15*, 591.
- (48) Moncton, D. E.; Axe, J. D.; DiSalvo, F. J. Study of Superlattice Formation in 2H-NbSe₂ and 2H-TaSe₂ by Neutron Scattering. *Phys. Rev. Lett.* **1975**, *34*, 734–737.
- (49) Uchida, S.; Sugai, S. Infrared and Raman Studies on Commensurate CdW States in Transition Metal Dichalcogenides. *Physica B+C* **1981**, *105*, 393–399.
- (50) Lee, C.-H.; Lee, G.-H.; van der Zande, A. M.; Chen, W.; Li, Y.; Han, M.; Cui, X.; Arefe, G.; Nuckolls, C.; Heinz, T. F.; Guo, J. Atomically Thin P-N Junctions with Van Der Waals Heterointerfaces. *Nat. Nanotechnol.* **2014**, *9*, 676–681.
- (51) Albertini, O. R.; Zhao, R.; McCann, R. L.; Feng, S.; Terrones, M.; Freericks, J. K.; Robinson, J. A.; Liu, A. Y. Zone-Center Phonons of Bulk, Few-Layer, and Monolayer 1T-TaS₂: Detection of Commensurate Charge Density Wave Phase through Raman Scattering. *Phys. Rev. B: Condens. Matter Mater. Phys.* **2016**, *93*, 214109.
- (52) Mattheiss, L. F. Band Structures of Transition-Metal-Dichalcogenide Layer Compounds. *Phys. Rev. B* **1973**, *8*, 3719–3740.
- (53) Zhang, W.; Li, Z.; Li, F.; Zhang, H.; Peng, J.; Tang, C.; Wang, Q.; He, K.; Chen, X.; Wang, L.; Ma, X. Interface Charge Doping Effects on Superconductivity of Single-Unit-Cell FeSe Films on SrTiO₃ Substrates. *Phys. Rev. B: Condens. Matter Mater. Phys.* **2014**, *89*, 060506.
- (54) Bang, J.; Li, Z.; Sun, Y. Y.; Samanta, A.; Zhang, Y. Y.; Zhang, W.; Wang, L.; Chen, X.; Ma, X.; Xue, Q. K.; Zhang, S. B. Atomic and Electronic Structures of Single-Layer FeSe on SrTiO₃(001): The Role of Oxygen Deficiency. *Phys. Rev. B: Condens. Matter Mater. Phys.* **2013**, *87*, 220503.
- (55) Qian, D.; Hsieh, D.; Wray, L.; Morosan, E.; Wang, N. L.; Xia, Y.; Cava, R. J.; Hasan, M. Z. Emergence of Fermi Pockets in a New Excitonic Charge-Density-Wave Melted Superconductor. *Phys. Rev. Lett.* **2007**, *98*, 117007.
- (56) Li, Y.; Duerloo, K.-A. N.; Wauson, K.; Reed, E. J. Structural Semiconductor-to-Semimetal Phase Transition in Two-Dimensional Materials Induced by Electrostatic Gating. *Nat. Commun.* **2016**, *7*, 10671.
- (57) Kim, J.-J.; Park, C.; Yamaguchi, W.; Shiino, O.; Kitazawa, K.; Hasegawa, T. Observation of a Phase Transition from the T Phase to the H Phase Induced by a Stm Tip in 1T-TaS₂. *Phys. Rev. B: Condens. Matter Mater. Phys.* **1997**, *56*, R15573–R15576.